EINDHOVEN UNIVERSITY OF TECHNOLOGY

Area-Selective Atomic Layer Deposition of Two-Dimensional WS2 Nanolayers

Citation for published version (APA):
Balasubramanyam, S., Merkx, M. J. M., Verheijen, M. A., Kessels, W. M. M., Mackus, A. J. M., & Bol, A. A. (2020). Area-Selective Atomic Layer Deposition of Two-Dimensional WS2 Nanolayers. *ACS Materials Letters*, *2*(5), 511-518. https://doi.org/10.1021/acsmaterialslett.0c00093

DOI:
10.1021/acsmaterialslett.0c00093

Document status and date:
Published: 04/05/2020

Document Version:
Accepted manuscript including changes made at the peer-review stage

Please check the document version of this publication:

• A submitted manuscript is the version of the article upon submission and before peer-review. There can be important differences between the submitted version and the official published version of record. People interested in the research are advised to contact the author for the final version of the publication, or visit the DOI to the publisher's website.
• The final author version and the galley proof are versions of the publication after peer review.
• The final published version features the final layout of the paper including the volume, issue and page numbers.

Link to publication

General rights
Copyright and moral rights for the publications made accessible in the public portal are retained by the authors and/or other copyright owners and it is a condition of accessing publications that users recognise and abide by the legal requirements associated with these rights.

• Users may download and print one copy of any publication from the public portal for the purpose of private study or research.
• You may not further distribute the material or use it for any profit-making activity or commercial gain
• You may freely distribute the URL identifying the publication in the public portal.

If the publication is distributed under the terms of Article 25fa of the Dutch Copyright Act, indicated by the “Taverne” license above, please follow below link for the End User Agreement:

www.tue.nl/taverne

Take down policy
If you believe that this document breaches copyright please contact us at:

openaccess@tue.nl

providing details and we will investigate your claim.

Download date: 22. May. 2024

Area-selective atomic layer deposition of 2D WS_2 nanolayers

Shashank Balasubramanyam[1], Marc J. M. Merkx[1], Marcel A. Verheijen[1,2], Wilhelmus M. M. Kessels[1], Adriaan J. M. Mackus[1] and Ageeth A. Bol[1,*]

[1]Department of Applied Physics, Eindhoven University of Technology, 5600 MB Eindhoven, The Netherlands

[2]Eurofins Materials Science Netherlands B.V., High Tech Campus 11, 5656 AE Eindhoven, The Netherlands

*(a.a.bol@tue.nl)

Abstract

With downscaling of device dimensions, two dimensional (2D) semiconducting transition metal dichalcogenides (TMDs) such as WS_2 are being considered as promising materials for future applications in nanoelectronics. However, at these nanoscale regimes, incorporating TMD layers in the device architecture with precise control of critical features is challenging using current top-down processing techniques. In this contribution, we pioneer the combination of two key avenues in atomic-scale processing: area-selective atomic layer deposition (AS-ALD) and growth of 2D materials and demonstrate bottom-up processing of 2D WS_2 nanolayers. Area-selective deposition of WS_2 nanolayers is enabled using a *ABC-type* plasma-enhanced ALD process involving acetylacetone (Hacac) as inhibitor (A), bis*(tert*-butylimido)-bis(dimethylamido)-tungsten as precursor (B), and H_2S plasma as the co-reactant (C) at a low deposition temperature of 250 °C. The developed AS-ALD process results in the immediate growth of WS_2 on SiO_2 while effectively blocking growth on Al_2O_3 as confirmed by *in situ* spectroscopic ellipsometry and *ex situ* X-ray photoelectron spectroscopy measurements. As a proof of concept, the AS-ALD process is demonstrated on patterned Al_2O_3/SiO_2 surfaces. The AS-ALD WS_2 films exhibited sharp Raman (E_{2g}^1 and A_{1g}) peaks on SiO_2, a fingerprint of crystalline WS_2 layers, upon annealing at temperatures within the thermal budget of semiconductor back-end-of-line processing (≤ 450 °C). Our AS-ALD process also allows selective growth on various TMDs and transition metal oxides while blocking growth on HfO_2 and TiO_2. It is expected that this work will lay the foundation for area-selective ALD of other 2D materials.

The downscaling of dimensions in nanoelectronic devices has led to the exploration of alternate, two dimensional (2D) semiconductors for future nanodevice applications.[1–6] In this regard, semiconducting transition metal dichalcogenides (TMDs) such as WS_2 have attracted a lot of interest due to their high carrier mobility and direct bandgap in the monolayer regime.[3,7] In ultra-scaled nanoelectronic devices, it is crucial to precisely incorporate TMD layers at desired locations in the device architecture with consistent layer characteristics. Conventionally, lithography-based top-down processing techniques are used to pattern films into device features. Precise patterning and alignment of critical device features will become challenging using the current top-down processing schemes especially in sub-5 nm technology nodes.[8–10] At the same time, patterning 2D TMD layers with resist-based lithography risks inducing contaminants into the layers, that can significantly impact their functional characteristics.[11–14] In this regard, selective-growth of TMD layers on predetermined locations (also referred to as area-selective deposition) via bottom-up approaches has attracted significant interest from both academia and industry.[14] Rather than performing deposition, lithography and etching for each layer in a device stack, some of the layers can be incorporated in a bottom-up manner using this approach. By directly depositing TMD layers on pre-patterned surfaces, area-selective deposition can enable the integration of TMD layers in multilayer device stacks without the need for resist-based patterning of the delicate TMD layers. Therefore, this approach decreases the total number of lithography and etching steps in the fabrication of nanoelectronic devices, and thus, can enable cost-effective device fabrication schemes for future technology nodes.

Area-selective deposition of TMD layers has been sparingly reported in the literature. Flakes of MoS_2 have been deposited at pre-determined locations by using lithography patterned nucleation seeds or topological features in chemical vapour deposition (CVD) processes.[15,16] In these reported methods, the removal of seeds after fabrication is not straightforward.[14,17] The control over thickness and shape of the seeded TMD structures is also a point of concern.[17] Area-selective growth of CVD MoS_2 has also been enabled by enhancing the reactivity of pre-determined areas to CVD surface reactions through chemical treatments[17] and mechanically induced triboelectric effects.[14] The use of seed layers were mitigated in these processes. However, the longevity and stability of the enhanced surface reactivity of pre-determined areas is uncertain with these methods. Gallium ion beams have been used to control the density of surface hydroxyl groups on the initial substrate (SiO_2) and achieve patterned growth of MoS_2 in a CVD process.[18] Recently, WS_2 was selectively deposited using pre-patterned a-Si sacrificial layers in a pulsed CVD process.[19] Conceivably, to date, area-selective growth of TMD layers has been restricted to CVD-based processes[14–16] that typically involve high temperature processing (≥700 °C). Moreover, these methods do not necessarily offer atomic level-thickness control over the TMD layer being deposited.

Recently, area-selective atomic layer deposition (AS-ALD) has attracted a lot of attention as a promising alternative pathway to realize selective growth of materials on pre-determined locations.[20,21] AS-ALD is an advanced atomic layer deposition (ALD) process that limits growth to pre-determined areas by taking advantage of the surface chemistry differences between the growth and non-growth areas.[22,23] The chemospecific characteristic of the process coupled with the atomic level accuracy of ALD is exploited to enable bottom-up growth of materials at precise locations without requiring any additional patterning of the film being deposited.[20,22,24] To date, especially AS-ALD of metals[21,25–30] and dielectrics[21,23,31] has been reported in the literature. These studies are being considered promising in terms of patterning ALD grown films for applications in nanoelectronics[22,32,33] and catalysis.[34,35] Area-selective

ALD of 2D TMD layers has however, remained unexplored. Ideally, an AS-ALD process should enable area-selective growth and at the same time offer the merits of conventional ALD processes including angstrom-level thickness control, uniform and conformal film growth over large-area substrates and high aspect ratio 3D structures, and low-temperature processing (typically $T \leq 450$ °C).[36–41] Therefore, there is considerable interest in developing AS-ALD processes for selectively depositing TMD layers.

Selective growth via AS-ALD can be realized by deactivating the non-growth area for a specific ALD chemistry.[20,21] Select areas of the substrate can be functionalized with a blocking layer that allows growth only on the non-functionalized areas of the substrate.[20] Self-assembled monolayers (SAMs) and small inhibitor molecules have been investigated as blocking agents in AS-ALD processes. Recently, Mameli et al. showcased the efficacy of vapour-phase dosed acetylacetonate inhibitor molecules (referred to as Hacac) in blocking precursor adsorption and thereby, blocking film growth on Al_2O_3 surfaces during AS-ALD of SiO_2.[23] The Hacac molecules were dosed every cycle unlike the one time application of SAMs in other AS-ALD processes, which makes the approach compatible with a wider range of processes including plasma-enhanced ALD (PEALD). Taking a cue from these results, in this work, we use Hacac as inhibitor to selectively deposit mono-to-multilayers of WS_2. Selective growth was realized on (1) SiO_2 (commonly used substrate for the growth of 2D TMD layers), (2) 2D TMDs such as MoS_2, NbS_2, and TiS_2 and (3) transition metal oxides such as MoO_3, Nb_2O_5 and WO_3 while effectively blocking growth on Al_2O_3 and HfO_2 surfaces at a low deposition temperature of 250 °C. We expect this first AS-ALD process for 2D-WS_2 to enable exploration of area-selective ALD processes for other functional 2D materials.

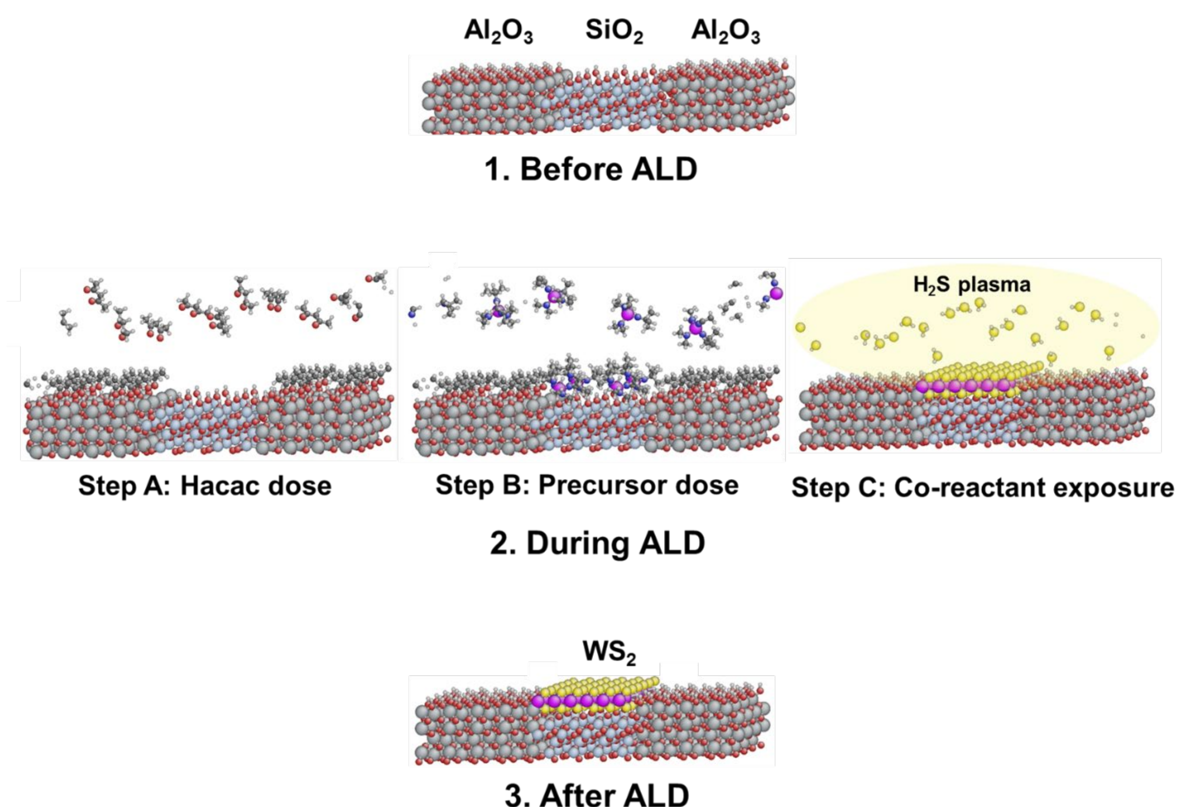

Figure 1. Schematic illustration of the WS_2 area-selective ALD process using *ABC-type* ALD cycles. The Al_2O_3/SiO_2 patterned surface is shown before, during, and after ALD. The individual ALD steps of the *ABC-type* ALD cycle are indicated: Step A – Hacac dose, Step B – bis(*tert*-butylimido)-bis(dimethylamido)-tungsten precursor dose, and Step C – H_2S plasma exposure. Using this process, WS_2 is selectively deposited on SiO_2 in presence of Al_2O_3.

A schematic of our AS-ALD approach is shown in Figure 1 for pre-patterned Al_2O_3 (non-growth area) and SiO_2 (growth area) surfaces. It is based on a three-step (i.e. *ABC-type*) ALD process. In step A, we dose Hacac molecules that adsorb only on the Al_2O_3 surface and not on the SiO_2 surface. In step B, the precursor adsorption is blocked by the adsorbed Hacac inhibitor molecules on the Al_2O_3 surface, while the tungsten precursor (bis(*tert*-butylimido)-bis(dimethylamido)-tungsten) readily adsorbs on the SiO_2 surface. In the final step C, the H_2S plasma functions as the ALD co-reactant enabling the growth of WS_2 on SiO_2. On the Al_2O_3 surface, it removes the adsorbed inhibitor molecules from the Al_2O_3 surface. Such ALD cycles are repeated to selectively deposit WS_2 films on SiO_2 surfaces. The BC steps of the ABC cycles used in this work were adopted from our previously reported WS_2 ALD process which resulted in the growth of WS_2 films.[42]

Figure 2a shows the nucleation curves for the *ABC-type* WS_2 ALD process on SiO_2 (growth area) and Al_2O_3 (non-growth area), as-determined from *in situ* spectroscopic ellipsometry (SE). The plot shows that WS_2 grows readily on SiO_2 surfaces without any growth delay. The film thickness increases linearly with number of ALD cycles, a characteristic of the ALD growth behaviour, with a growth per cycle (GPC) of ~0.6 Å. On the other hand, for the same *ABC-type* WS_2 ALD process on Al_2O_3, a growth delay of ~20 ALD cycles is observed. These results indicate that ~1 nm of WS_2 (at least one monolayer) can be selectively deposited on SiO_2 while blocking the growth on Al_2O_3. When performing BC cycles (without the use of Hacac), no

growth delay was observed on Al_2O_3 as evidenced by a linear increase in thickness with the number of ALD cycles (Figure S1).

The nucleation behaviour of our process was corroborated with XPS measurements (Figure 2b-c). In line with the *in situ* SE data, the integrated area of the XPS W4f peaks increased linearly with number of ALD cycles on SiO_2,while a growth delay of ~20 ALD cycles was observed on Al_2O_3 (see Figure S2a-d for W and S XPS peak evolution). As shown in Figure 2c, distinct W4f doublet peaks corresponding to WS_2 (W^{+4} oxidation state, binding energy = ~32.1 eV and ~34.2 eV) were observed on the SiO_2 surface, whereas no W4f core level (W^{+4}) signals were observed on the Al_2O_3 surface after 20 ALD cycles. Note that the XPS detection limit for W on top of SiO_2 and Al_2O_3 was estimated to be below 0.01 monolayer or ~ 2 x 10^{12} atoms/cm^2.[43] A film stoichiometry (S:W) of 2.3 was determined from XPS measurements on SiO_2 similar to our previous work.[42] The binding energy of the XPS W4f core levels ($W4f_{7/2}$ and $W4f_{5/2}$) appears to match those commonly observed for the 1*T* phase of WS_2.[44] However, we have previously[42] established the growth of 2*H* phase of WS_2 layers for the same ALD process at a similar temperature (at 300 °C using XRD measurements). So we expect these layers to be in 2*H* phase.

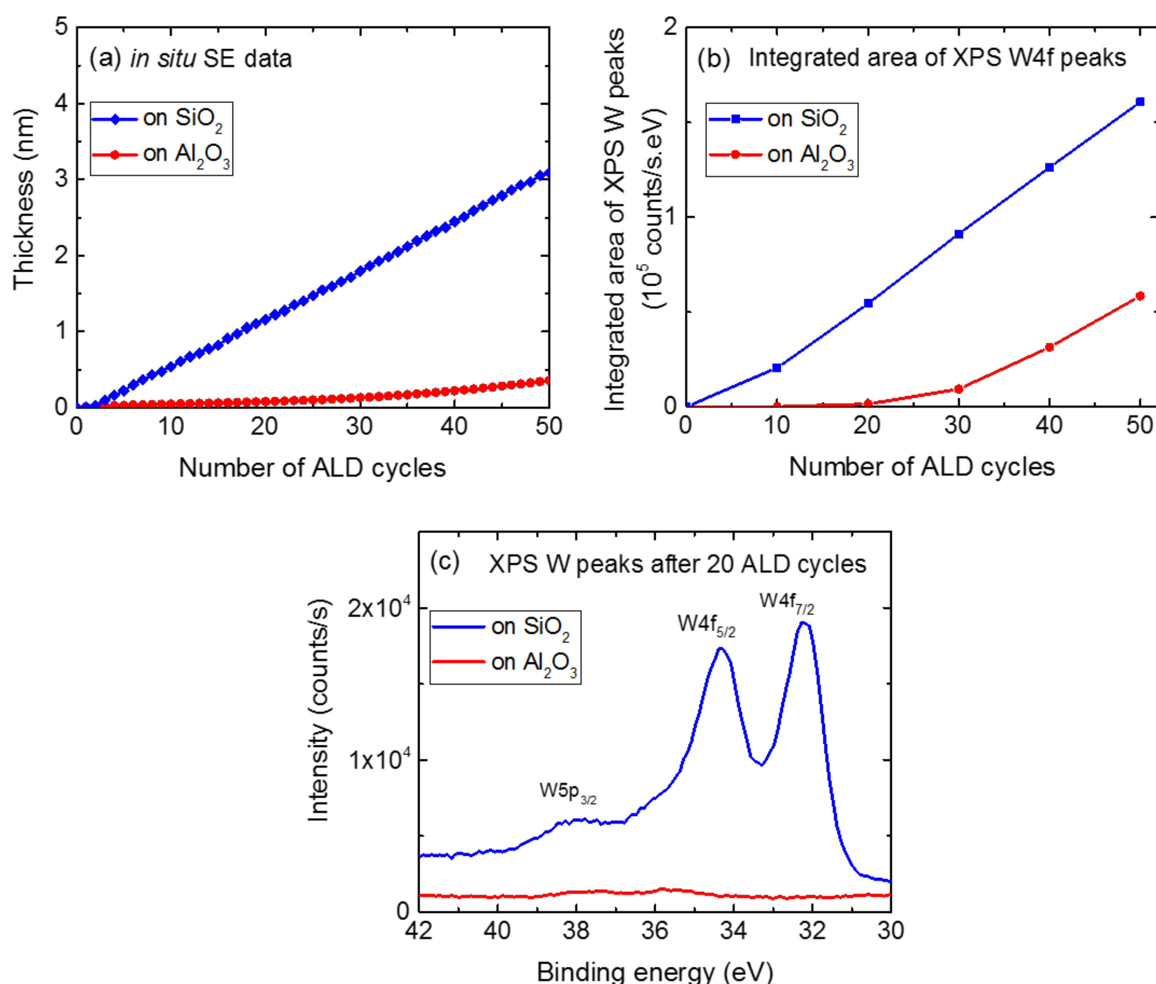

Figure 2. (a) Film thickness as a function of number ALD cycles for the *ABC-type* WS_2 process on SiO_2 (growth area) and Al_2O_3 (non-growth area), as determined from *in situ* SE. (b) The integrated area of XPS W peaks after various number of ALD cycles determined for the Al_2O_3 and SiO_2 surfaces. (c) Raw

XPS spectra of the W4f core level after 20 ALD cycles on the Al_2O_3 and SiO_2 surfaces. XPS measurements were performed on samples deposited at 250 °C.

On SiO_2, the adsorption of Hacac molecules is known to be very minimal relative to Al_2O_3[23] and in line with this, no growth delay was observed in this work as discussed above (Figure 2a,b). Furthermore, XPS depth profiling of the WS_2 films revealed no carbon impurity incorporation from Hacac molecules (Figure S2e). These results confirm that the addition of Hacac (step A) to the WS_2 ALD process (steps B, C) does not influence the WS_2 deposition on a SiO_2 starting surface and on the WS_2 itself. Therefore, our process can be used to selectively deposit pure WS_2 (~2 monolayers) with angstrom-level thickness control on SiO_2 in presence of Al_2O_3.

To quantify the area-selectivity of our process, we use the accepted definition of selectivity in the field of area-selective deposition[45,46]:

$$selectivity = \frac{\theta_{GA} - \theta_{NGA}}{\theta_{GA} + \theta_{NGA}}$$

where, θ_{GA} and θ_{NGA} represent the amount of material present (WS_2 in this case) on the growth and non-growth areas, respectively. Using this definition, the selectivity of the *ABC-type* WS_2 ALD process was calculated using the number of W XPS counts in Figure 2b. After 20 ALD cycles, a high selectivity value of ~0.95 was obtained. This corresponds to a selective deposition of WS_2 with a thickness of ~1nm, which is more than one monolayer (one monolayer of WS_2 ~0.65 nm). After 30 cycles, the selectivity was determined to be ~0.82. This corresponds to a selective deposition of ~3 monolayers of WS_2. With increasing number of ALD cycles, the selectivity starts to decrease drastically (0.45 after 50 ALD cycles). The loss in selectivity primarily arises from ineffective blocking of precursor adsorption by Hacac with increasing number of ALD cycles. A degraded blocking of the precursor adsorption can occur due to the introduction of surface defects that influence Hacac adsorption negatively and/or incomplete Hacac coverage that allows the precursor molecules to access certain surface reactive sites.[23]

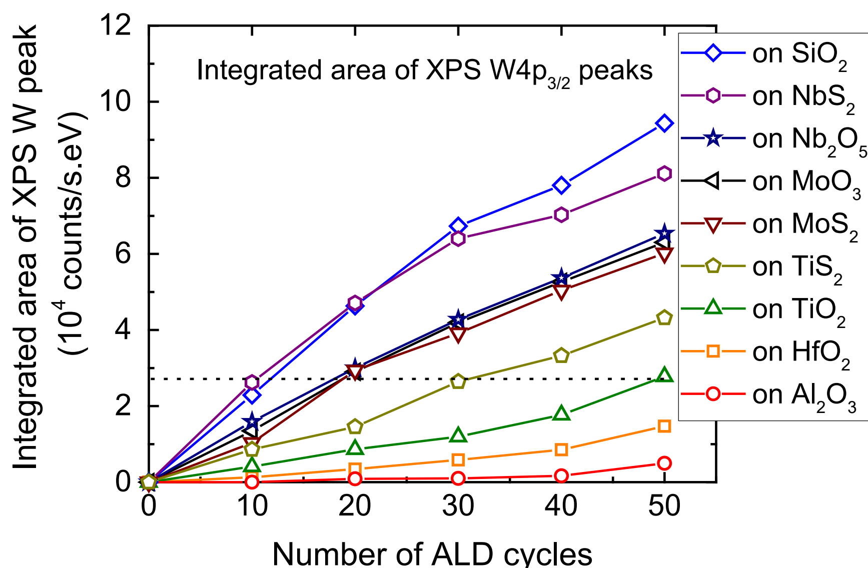

Figure 3. Integrated area of XPS $W4p_{3/2}$ peaks as a function of number ALD cycles for the *ABC-type* WS_2 process on various starting surfaces. The dotted black line serves as a reference to the integrated area of XPS $W4p_{3/2}$ peak (2.7 x 10^4 counts/s.eV) corresponding to a monolayer of WS_2 deposited on SiO_2 (prepared using ~12 ALD cycles, Figure 2a).

To explore the versatility of our process on various surfaces, the ABC-type WS_2 ALD cycles were performed on several starting surfaces including TMDs and transition metal oxides as shown in Figure 3. The integrated area of the XPS $W4p_{3/2}$ peaks on these surfaces were used to compare the ALD growth. The $W4p_{3/2}$ peaks were used for establishing the nucleation curves in Figure 3 instead of the W4f peaks as the W4f peaks overlaps with some of the elemental XPS peaks of the surface constituents (e.g. $Hf5p_{3/2}$ and $Ti3p_{3/2}$, Figure S3). Among various starting surfaces investigated, a growth delay of ~10 ALD cycles was observed on HfO_2 (Figure 3). Even after 50 ALD cycles, the integrated $W4p_{3/2}$ peak area was significantly lower on HfO_2 when compared to the peak area determined for a monolayer of WS_2 deposited on SiO_2 (dotted black line). The integrated $W4p_{3/2}$ peak area was observed to be also significantly lower on TiO_2. On the other hand, characteristic XPS $W4p_{3/2}$ peaks with relatively large integrated peak areas were observed on 2D TMDs including MoS_2, NbS_2, and TiS_2 starting surfaces, which indicated WS_2 film growth without any significant growth delay. As WS_2 grows readily on several TMDs surfaces, our process can be also used to selectively grow 2D TMD vertical heterostructures (e.g., WS_2 on MoS_2) in presence of the non-growth areas (i.e. Al_2O_3 and HfO_2). Immediate film growth was also observed on transition metal oxides such as MoO_3 and Nb_2O_5 surfaces.

Raman spectroscopy is a widely used technique to establish and characterize the growth of crystalline TMD layers. Raman measurements revealed that our as-deposited AS-ALD WS_2 films on SiO_2 at 250° C were amorphous in nature as signature WS_2 Raman fingerprints were not observed. Cross-section TEM images (Figure S4a) indicated the growth of an amorphous WS_2 film matrix embedded with nano-crystalline regions. The growth mechanism for ALD MX_2 layers (both crystalline and amorphous) is not well understood in the literature. In our work, we believe, the growth mechanism for amorphous WS_2 layers is expected to occur similar to that of crystalline WS_2 layers with the exception of long-range ordering of the layers. A model for the WS_2 crystalline film growth during plasma-ALD is described in our previous works.[42,47] The growth mode in amorphous WS_2 films (layer by layer or island growth *etc.*) could vary depending upon the processing conditions and the defects present on the growth surface.

In order to improve the crystallinity of WS_2 layers, the samples were annealed at 450 °C in a H_2S gas atmosphere for 30 min in the same ALD reactor (pressure during annealing = 300 mTorr). WS_2 is considered as a promising material for applications such as low-power devices in the back-end-of-line (BEOL).[3] Hence, the films were annealed within the thermal budget of BEOL compatible processing (≤ 450°C). Upon annealing, signature Raman vibration modes for crystalline WS_2 were observed on SiO_2 (Figure 4b). The two characteristic Raman modes at 356 cm^{-1} and 418 cm^{-1} wavenumbers correspond to the WS_2 in-plane (E_{2g}^1) and out-of-plane (A_{1g}) vibrations.[48–50] Cross-section TEM imaging (Figure S4b) showed a significant improvement in the crystallinity of the WS_2 layers upon annealing. The approximate grain size was ~10 nm as deduced from top-view TEM (Figure S4c and d). A detailed study on the fabrication and characterization of electronic devices such as filed effect transistors (FETs) using the annealed WS_2 layers (including temperature dependent resistivity measurements) will

be performed in a separate study. The root mean square (rms) surface roughness of the WS_2 films increased from ~0.1 to ~0.4 nm upon annealing, as-determined from AFM measurements (Figure S5). No Raman peaks were observed after performing WS_2 *ABC* cycles on Al_2O_3 as expected (Figure 4b).

As a proof-of-concept, we tested our *ABC-type* AS-ALD process on patterned Al_2O_3/SiO_2 surfaces. ALD grown Al_2O_3 was patterned on ALD grown SiO_2 (Figure 4a) using a regular lift-off process. After performing 20 ALD cycles, the patterned samples were annealed at 450 °C in a H_2S atmosphere. Raman spectroscopy line scans were performed to investigate the selectivity over the patterned surfaces. The line scan of the E^1_{2g} Raman mode over the patterned surface revealed very clear and sharp transitions at the SiO_2-Al_2O_3 interfaces with steep slopes (Figure 4c).

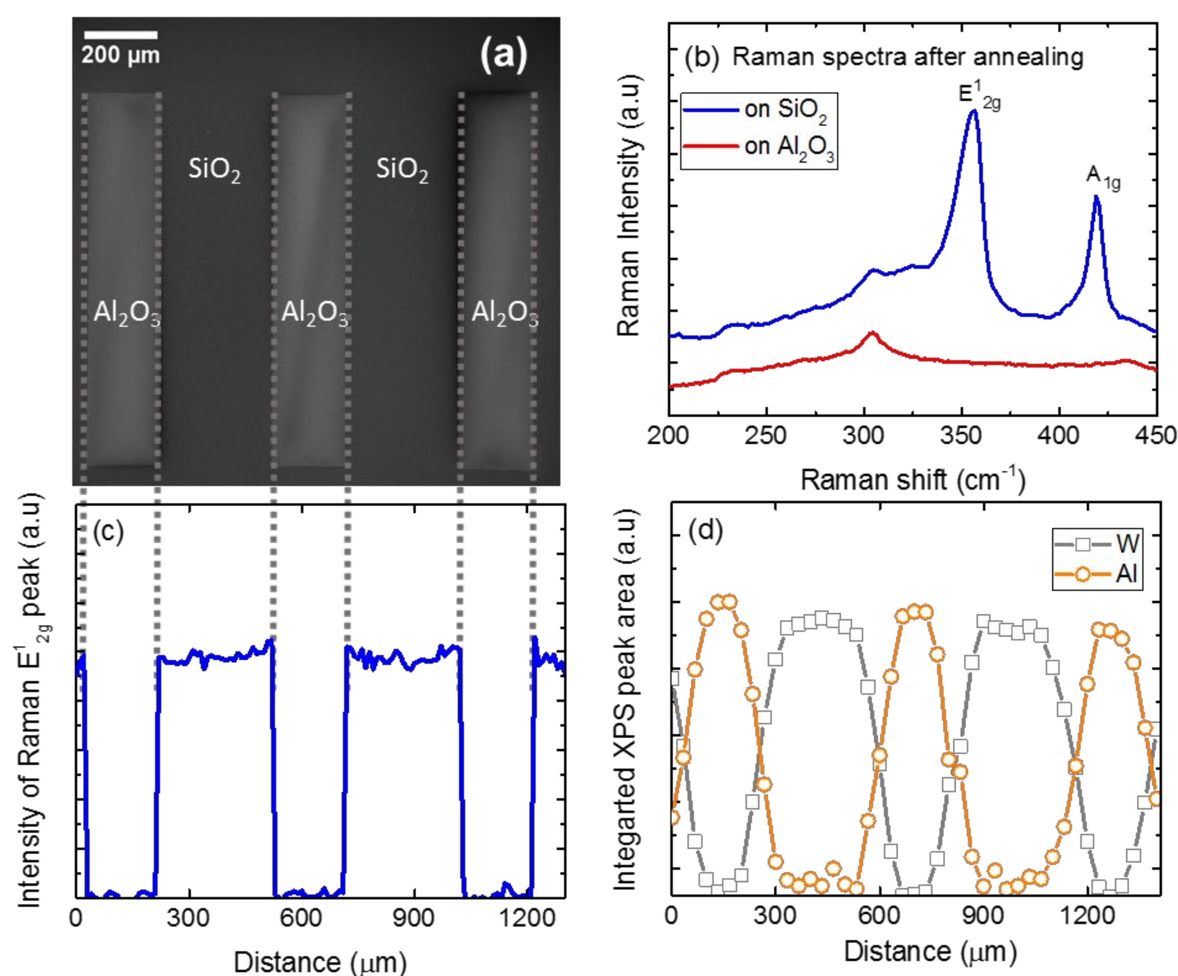

Figure 4. (a) Scanning electron microscopy (SEM) images of the Al_2O_3/SiO_2 patterned samples. (b) Raman spectra showing the characteristic in-plane (E^1_{2g}) and out-of-plane (A_{1g}) Raman modes of WS_2 on SiO_2 after annealing at 450 °C and (c) the corresponding Raman E^1_{2g} peak intensity line scans over the Al_2O_3/SiO_2 patterned samples after 20 *ABC-type* WS_2 ALD cycles. (d) XPS elemental W and Al line scans after 20 *ABC-type* WS_2 ALD cycles on the Al_2O_3/SiO_2 patterned samples.

XPS line scans were also performed on the annealed patterns to investigate the selectivity (see Figure S6 for XPS W4f core level spectra). The XPS line scans in Figure 4d show strong W

signals in the SiO_2 regions whereas, no W signals were observed in the Al_2O_3 regions. The overlap of the W and Al line scans at the interface can be attributed to the large spot size of the X-ray beam (~70 μm), which is comparable to the region of overlap and much larger than the spot size of the Raman laser (~5 μm).

In conclusion, we have demonstrated the area-selective deposition of 2D WS_2 nanolayers using ALD in a bottom-up processing approach. AS-ALD of WS_2 was achieved using an acetylacetone (Hacac) inhibitor (A), bis(*tert*-butylimido)-bis(dimethylamido)-tungsten precursor (B), and H_2S plasma (C) pulses in an *ABC-type* ALD process at a low deposition temperature of 250 °C. With this approach, WS_2 nanolayers are readily deposited on SiO_2, various 2D TMDs and transition metal oxides, while growth on Al_2O_3 and HfO_2 surfaces is effectively blocked. On the growth areas, pure WS_2 is deposited with angstrom-level thickness control. The AS-ALD WS_2 films exhibited sharp Raman peaks, a fingerprint of crystalline film growth, upon annealing at BEOL compatible temperatures (≤450 °C). As a proof of concept, the AS-ALD process has been demonstrated on patterned Al_2O_3/SiO_2 surfaces. Raman line scans over the SiO_2/Al_2O_3 patterns showed very sharp peak intensity transitions at the interface. The selectivity of our process was quantified and after 20 ALD cycles (at least one monolayer) a high selectivity of 0.95 is obtained. The results obtained in this work can be used as a platform to further explore the area-selective deposition of other 2D TMD materials.

EXPERIMENTAL PROCEDURES

All depositions were performed in a commercial FlexAL ALD reactor from Oxford Instruments. In essence, the reaction chamber is equipped with a remote inductively coupled plasma (ICP) source, a 200 mm substrate table, and a turbo molecular pump which enables a base pressure of 10^{-6} Torr. The reaction chamber wall temperature was set to 150 °C (maximum possible value) and the substrate table temperature was set to 250 °C. With these settings, the substrate temperature was estimated to be ~200 °C using a thermocouple on reference samples. The mismatch between the set and the estimate temperature can arise from limited contact in vacuum. Table S1 compares the set temperature (referred to as deposition temperature) and estimated temperatures. Throughout this work, deposition temperatures are used for discussion. The WS_2 AS-ALD process was primarily tested and characterized on SiO_2 (growth area) and Al_2O_3 (non-growth area). Both SiO_2 and Al_2O_3 (~30 nm) were deposited on *c*-Si with 450 nm thermal oxide using well-established ALD processes. Other starting surfaces reported in this work (various 2D TMDs and transition metal oxides) were also deposited using ALD processes. All substrates were subjected to a 20 minute pre-heating step in a 200 mTorr Ar environment to stabilize the substrate temperature. The substrates were then subjected to a H_2 plasma for 5 minutes prior to the AS-ALD process. The H_2 plasma power was set to 500 W and the pressure in the chamber was maintained at 50 mTorr. The following optimized exposures were used in our PEALD recipe: 3 pulses of 5 s each for the Hacac dose (Step A), 10 s for the bis(*tert*-butylimido)-bis(dimethylamido)-tungsten precursor dose (Step B), and 60 s for the H_2S plasma exposure (Step C). The Hacac inhibitor (Sigma Aldrich, ≥99% purity) was stored in a canister at room temperature and was vapour drawn into the reaction chamber. The two-step (*BC*) WS_2 PEALD recipe employing the tungsten precursor and H_2S plasma pulses reported in our previous work was used as a starting point to deposit WS_2 films.[42] The growth inhibition on Al_2O_3 and thereby, the selectivity of our process was observed to be significantly dependent on ALD processing conditions including H_2S plasma exposure time, H_2 plasma pre-treatment of Al_2O_3 and deposition temperature. This is further described in the supporting information

(Figure S7 and S8). Frequent usage of H_2S plasma exposures beyond 60 s led to flaking of deposited material on the substrate table. Thus, H_2S plasma exposures were seemingly limited to 60 s during most of our processing.

In situ spectroscopic ellipsometry (SE) was used to measure the apparent WS_2 film thickness using a B-spline function or Cauchy-based parametrization to model the experimental SE data. All *in situ* SE measurements were performed using a J.A. Woollam M2000F ellipsometer. X-ray photoelectron spectroscopy (XPS) was used to detect the presence of W on SiO_2 and Al_2O_3 surfaces. The XPS detection limit for W on top of SiO_2 and Al_2O_3 was determined to be below ~0.01 monolayer (~2×10^{12} atoms/cm^2).[43] All XPS studies were carried out using a Thermo Scientific KA1066 spectrometer with monochromatic Al Kα X-ray source ($h\nu$ = 1486.6 eV). The spot size of the incident X-rays was ~70 µm. XPS data analysis was carried out using the Avantage XPS software.

Scanning electron microscopy (SEM) images were obtained using a Zeiss Sigma microscope with an in-column, secondary electron detector. The acceleration voltage of the electron beam was 2 keV. Raman spectroscopy was performed to investigate the characteristic vibrational modes in WS_2 films. High-angle annular dark field (HAADF) scanning transmission electron microscopy (STEM) images were obtained using a probe-corrected JEOL JEM-ARM200F transmission electron microscope (TEM) operated at 80 kV. For top-view STEM imaging, WS_2 layers were deposited on Si_3N_4 windows coated with 5 nm of ALD SiO_2. For cross-section TEM studies, WS_2 layers deposited on Si_3N_4 windows were coated with an additional SiO_2 protective layer on top. A focused ion beam was used to create a cross-sectional sample using the standard lift-out method. Raman spectra were obtained using a Renishaw Invia Raman microscope equipped with a 514 nm laser at a power of ~0.5 mW. The laser spot size was ~5 µm. Atomic force microscopy (AFM) measurements were performed using a NT-MDT Solver P47 AFM.

ASSOCIATED CONTENT

Supporting information

Film growth on Al_2O_3: With and without Hacac; XPS data: tungsten and sulfur peak evolution and depth profiling of the carbon peak; Overlap of XPS Ti and Hf peaks with W4f peaks; TEM measurements: as-deposited and annealed WS_2; AFM measurements: as-deposited and annealed WS_2; XPS W4f core-level spectra after annealing WS_2 sample; Set temperature vs estimated substrate temperature; Impact of processing conditions on the growth inhibition on Al_2O_3 surface.

AUTHOR INFORMATION

Corresponding Author

*Email: a.a.bol@tue.nl

Acknowledgements

This work has been supported by the European Research Council (Grant Agreement No. 648787-ALDof2DTMDs. The authors acknowledge the technical assistance offered by Cristian van Helvoirt, Jeroen van Gerwen and Martijn Dijstelbloem. They also thank Wijnand Dijkstra

for his support with the AFM measurements and Saravana Basuvalingam for preparation of Al_2O_3/SiO_2 patterns.

References

(1) Chhowalla, M.; Jena, D.; Zhang, H. Two-Dimensional Semiconductors for Transistors. *Nat. Rev. Mater.* **2016**, *1*, 16052. https://doi.org/10.1038/natrevmats.2016.52.

(2) Fiori, G.; Bonaccorso, F.; Iannaccone, G.; Palacios, T.; Neumaier, D.; Seabaugh, A.; Banerjee, S. K.; Colombo, L. Electronics Based on Two-Dimensional Materials. *Nat. Nanotechnol.* **2014**, *9*, 768–779. https://doi.org/10.1038/nnano.2014.207.

(3) Schram, T.; Smets, Q.; Groven, B.; Heyne, M. H.; Kunnen, E.; Thiam, A.; Devriendt, K.; Delabie, A.; Lin, D.; Lux, M.; et al. WS_2 Transistors on 300 Mm Wafers with BEOL Compatibility. In *2017 47th European Solid-State Device Research Conference (ESSDERC)*; IEEE, **2017**, pp. 212–215. https://doi.org/10.1109/ESSDERC.2017.8066629.

(4) Yue, Y.; Chen, J.; Zhang, Y.; Ding, S.; Zhao, F.; Wang, Y.; Zhang, D.; Li, R.; Dong, H.; Hu, W.; et al. Two-Dimensional High-Quality Monolayered Triangular WS_2 Flakes for Field-Effect Transistors. *ACS Appl. Mater. Interfaces* **2018**, *10*, 22435–22444. https://doi.org/10.1021/acsami.8b05885.

(5) Cui, Y.; Xin, R.; Yu, Z.; Pan, Y.; Ong, Z.-Y.; Wei, X.; Wang, J.; Nan, H.; Ni, Z.; Wu, Y.; et al. High-Performance Monolayer WS_2 Field-Effect Transistors on High-κ Dielectrics. *Adv. Mater.* **2015**, *27*, 5230–5234. https://doi.org/10.1002/adma.201502222.

(6) Kumar, J.; Kuroda, M. A.; Bellus, M. Z.; Han, S.-J.; Chiu, H.-Y. Full-Range Electrical Characteristics of WS_2 Transistors. *Appl. Phys. Lett.* **2015**, *106*, 123508. https://doi.org/10.1063/1.4916403.

(7) Iqbal, M. W.; Iqbal, M. Z.; Khan, M. F.; Shehzad, M. A.; Seo, Y.; Park, J. H.; Hwang, C.; Eom, J. High-Mobility and Air-Stable Single-Layer WS_2 Field-Effect Transistors Sandwiched between Chemical Vapor Deposition-Grown Hexagonal BN Films. *Sci. Rep.* **2015**, *5*, 10699. https://doi.org/10.1038/srep10699.

(8) Schuegraf, K.; Abraham, M. C.; Brand, A.; Naik, M.; Thakur, R. Semiconductor Logic Technology Innovation to Achieve Sub-10 Nm Manufacturing. *IEEE J. Electron Devices Soc.* **2013**, *1*, 66–75. https://doi.org/10.1109/JEDS.2013.2271582.

(9) Thoms, S.; Macintyre, D. S.; Docherty, K. E.; Weaver, J. M. R. Alignment Verification for Electron Beam Lithography. *Microelectron. Eng.* **2014**, *123*, 9–12. https://doi.org/10.1016/j.mee.2014.02.005.

(10) Clark, R.; Tapily, K.; Yu, K.-H.; Hakamata, T.; Consiglio, S.; O’Meara, D.; Wajda, C.; Smith, J.; Leusink, G. Perspective: New Process Technologies Required for Future Devices and Scaling. *APL Mater.* **2018**, *6*, 058203. https://doi.org/10.1063/1.5026805.

(11) Amani, M.; Chin, M. L.; Mazzoni, A. L.; Burke, R. A.; Najmaei, S.; Ajayan, P. M.; Lou, J.; Dubey, M. Growth-Substrate Induced Performance Degradation in Chemically Synthesized Monolayer MoS_2 Field Effect Transistors. *Appl. Phys. Lett.* **2014**, *104*, 203506. https://doi.org/10.1063/1.4873680.

(12) Shao, P.-Z.; Zhao, H.-M.; Cao, H.-W.; Wang, X.-F.; Pang, Y.; Li, Y.-X.; Deng, N.-Q.; Zhang, J.; Zhang, G.-Y.; Yang, Y.; et al. Enhancement of Carrier Mobility in MoS_2 Field Effect Transistors by a SiO_2 Protective Layer. *Appl. Phys. Lett.* **2016**, *108*, 203105. https://doi.org/10.1063/1.4950850.

(13) Addou, R.; McDonnell, S.; Barrera, D.; Guo, Z.; Azcatl, A.; Wang, J.; Zhu, H.; Hinkle, C. L.; Quevedo-Lopez, M.; Alshareef, H. N.; et al. Impurities and Electronic Property Variations of Natural MoS_2 Crystal Surfaces. *ACS Nano* **2015**, *9*, 9124–9133. https://doi.org/10.1021/acsnano.5b03309.

(14) Ryu, B.; Li, D.; Park, C.; Rokni, H.; Lu, W.; Liang, X. Rubbing-Induced Site-Selective Growth of MoS_2 Device Patterns. *ACS Appl. Mater. Interfaces* **2018**, *10*, 43774–43784. https://doi.org/10.1021/acsami.8b15108.

(15) Han, G. H.; Kybert, N. J.; Naylor, C. H.; Lee, B. S.; Ping, J.; Park, J. H.; Kang, J.; Lee, S. Y.; Lee, Y. H.; Agarwal, R.; et al. Seeded Growth of Highly Crystalline Molybdenum Disulphide Monolayers at Controlled Locations. *Nat. Commun.* **2015**, *6*, 6128. https://doi.org/10.1038/ncomms7128.

(16) Sun, D.; Nguyen, A. E.; Barroso, D.; Zhang, X.; Preciado, E.; Bobek, S.; Klee, V.; Mann, J.; Bartels, L. Chemical Vapor Deposition Growth of a Periodic Array of Single-Layer MoS_2 Islands via Lithographic Patterning of an SiO_2/Si Substrate. *2D Mater.* **2015**, *2*, 045014. https://doi.org/10.1088/2053-1583/2/4/045014.

(17) Chen, X.; Park, Y. J.; Das, T.; Jang, H.; Lee, J.-B.; Ahn, J.-H. Lithography-Free Plasma-Induced Patterned Growth of MoS_2 and Its Heterojunction with Graphene. *Nanoscale* **2016**, *8*, 15181–15188. https://doi.org/10.1039/C6NR03318K.

(18) Bartolucci, S. F.; Kaplan, D.; Maurer, J. A. Ion Beam-Induced Hydroxylation Controls Molybdenum Disulfide Growth. *2D Mater.* **2017**, *4*, 021017. https://doi.org/10.1088/2053-1583/aa5e7e.

(19) Heyne, M. H.; de Marneffe, J.-F.; Delabie, A.; Caymax, M.; Neyts, E. C.; Radu, I.; Huyghebaert, C.; De Gendt, S. Two-Dimensional WS_2 Nanoribbon Deposition by Conversion of Pre-Patterned Amorphous Silicon. *Nanotechnology* **2017**, *28*, 04LT01. https://doi.org/10.1088/1361-6528/aa510c.

(20) Mackus, A. J. M.; Merkx, M. J. M.; Kessels, W. M. M. From the Bottom-Up: Toward Area-Selective Atomic Layer Deposition with High Selectivity. *Chem. Mater.* **2019**, *31*, 2–12. https://doi.org/10.1021/acs.chemmater.8b03454.

(21) Biyikli, N.; Haider, A.; Deminskyi, P.; Yilmaz, M. Self-Aligned Nanoscale Processing Solutions via Selective Atomic Layer Deposition of Oxide, Nitride, and Metallic Films. In *Low-Dimensional Materials and Devices 2017*; Kobayashi, N. P., Talin, A. A., Davydov, A. V., Islam, M. S., Eds.; SPIE, 2017; p 20. https://doi.org/10.1117/12.2276141.

(22) Mackus, A. J. M.; Bol, A. A.; Kessels, W. M. M. The Use of Atomic Layer Deposition in Advanced Nanopatterning. *Nanoscale* **2014**, *6*, 10941–10960. https://doi.org/10.1039/C4NR01954G.

(23) Mameli, A.; Merkx, M. J. M.; Karasulu, B.; Roozeboom, F.; Kessels, W. M. M.; Mackus, A. J. M. Area-Selective Atomic Layer Deposition of SiO_2 Using Acetylacetone as a Chemoselective Inhibitor in an ABC-Type Cycle. *ACS Nano* **2017**, *11*, 9303–9311. https://doi.org/10.1021/acsnano.7b04701.

(24) Mameli, A.; Karasulu, B.; Verheijen, M. A.; Barcones, B.; Macco, B.; Mackus, A. J. M.; Kessels, W. M. M. E.; Roozeboom, F. Area-Selective Atomic Layer Deposition of ZnO by Area Activation Using Electron Beam-Induced Deposition. *Chem. Mater.* **2019**, *31*, 1250–1257. https://doi.org/10.1021/acs.chemmater.8b03165.

(25) Shaw, J. R.; Chluba, J. Precise Cosmological Parameter Estimation Using CosmoRec. *Mon. Not. R. Astron. Soc.* **2011**, *415*, 1343–1354. https://doi.org/10.1111/j.1365-2966.2011.18782.x.

(26) Vos, M. F. J.; Chopra, S. N.; Verheijen, M. A.; Ekerdt, J. G.; Agarwal, S.; Kessels, W. M. M.; Mackus, A. J. M. Area-Selective Deposition of Ruthenium by Combining Atomic Layer Deposition and Selective Etching. *Chem. Mater.* **2019**, *31*, 3878–3882. https://doi.org/10.1021/acs.chemmater.9b00193.

(27) Vervuurt, R. H. J.; Sharma, A.; Jiao, Y.; Kessels, W. M. M.; Bol, A. A. Area-Selective Atomic Layer Deposition of Platinum Using Photosensitive Polyimide. *Nanotechnology* **2016**, *27*, 405302. https://doi.org/10.1088/0957-4484/27/40/405302.

(28) Lee, H.-B.-R.; Kim, H. Area Selective Atomic Layer Deposition of Cobalt Thin Films. In *ECS Transactions*; ECS, **2008**, 16, 219–225. https://doi.org/10.1149/1.2979997.

(29) Mackus, A. J. M.; Mulders, J. J. L.; van de Sanden, M. C. M.; Kessels, W. M. M. Local Deposition of High-Purity Pt Nanostructures by Combining Electron Beam Induced Deposition and Atomic Layer Deposition. *J. Appl. Phys.* **2010**, *107*, 116102. https://doi.org/10.1063/1.3431351.

(30) Bobb-Semple, D.; Nardi, K. L.; Draeger, N.; Hausmann, D. M.; Bent, S. F. Area-Selective Atomic Layer Deposition Assisted by Self-Assembled Monolayers: A Comparison of Cu, Co, W, and Ru. *Chem. Mater.* **2019,** *31*, 1635-1645. https://doi.org/10.1021/acs.chemmater.8b04926.

(31) Seo, S.; Yeo, B. C.; Han, S. S.; Yoon, C. M.; Yang, J. Y.; Yoon, J.; Yoo, C.; Kim, H.; Lee, Y.; Lee, S. J.; et al. Reaction Mechanism of Area-Selective Atomic Layer Deposition for Al_2O_3 Nanopatterns. *ACS Appl. Mater. Interfaces* **2017**, *9*, 41607–41617. https://doi.org/10.1021/acsami.7b13365.

(32) Sinha, A.; Hess, D. W.; Henderson, C. L. Area-Selective ALD of Titanium Dioxide Using Lithographically Defined Poly(Methyl Methacrylate) Films. *J. Electrochem. Soc.* **2006**, *153*, G465. https://doi.org/10.1149/1.2184068.

(33) Park, K. J.; Doub, J. M.; Gougousi, T.; Parsons, G. N. Microcontact Patterning of Ruthenium Gate Electrodes by Selective Area Atomic Layer Deposition. *Appl. Phys. Lett.* **2005**, *86*, 051903. https://doi.org/10.1063/1.1852079.

(34) Cao, K.; Cai, J.; Liu, X.; Chen, R. Review Article: Catalysts Design and Synthesis via Selective Atomic Layer Deposition. *J. Vac. Sci. Technol. A Vacuum, Surfaces, Film.* **2018**, *36*, 010801. https://doi.org/10.1116/1.5000587.

(35) O'Neill, B. J.; Jackson, D. H. K.; Lee, J.; Canlas, C.; Stair, P. C.; Marshall, C. L.; Elam, J. W.; Kuech, T. F.; Dumesic, J. A.; Huber, G. W. Catalyst Design with Atomic Layer Deposition. *ACS Catal.* **2015**, *5*, 1804–1825. https://doi.org/10.1021/cs501862h.

(36) Mattinen, M.; Hatanpää, T.; King, P. J.; Meinander, K.; Mizohata, K.; Jalkanen, P.; Räisänen, J.; Ritala, M.; Leskelä, M. Crystalline Tungsten Sulfide Thin Films by Atomic Layer Deposition and Mild Annealing. *J. Vac. Sci. Technol. A* **2019**, *37*,

020921. https://doi.org/10.1116/1.5074153.

(37) Hao, W.; Marichy, C.; Journet, C. Atomic Layer Deposition of Stable 2D Materials. *2D Mater.* **2018**, *6*, 012001. https://doi.org/10.1088/2053-1583/aad94f.

(38) Groven, B.; Heyne, M.; Nalin Mehta, A.; Bender, H.; Nuytten, T.; Meersschaut, J.; Conard, T.; Verdonck, P.; Van Elshocht, S.; Vandervorst, W.; et al. Plasma-Enhanced Atomic Layer Deposition of Two-Dimensional WS_2 from WF_6, H_2 Plasma, and H_2S. *Chem. Mater.* **2017**, *29*, 2927–2938. https://doi.org/10.1021/acs.chemmater.6b05214.

(39) Jurca, T.; Moody, M. J.; Henning, A.; Emery, J. D.; Wang, B.; Tan, J. M.; Lohr, T. L.; Lauhon, L. J.; Marks, T. J. Low-Temperature Atomic Layer Deposition of MoS_2 Films. *Angew. Chemie Int. Ed.* **2017**, *56*, 4991–4995. https://doi.org/10.1002/anie.201611838.

(40) George, S. M. Atomic Layer Deposition: An Overview. *Chem. Rev.* **2010**, *110*, 111–131. https://doi.org/10.1021/cr900056b.

(41) Puurunen, R. L. Surface Chemistry of Atomic Layer Deposition: A Case Study for the Trimethylaluminum/Water Process. *J. Appl. Phys.* **2005**, *97*, 121301. https://doi.org/10.1063/1.1940727.

(42) Balasubramanyam, S.; Shirazi, M.; Bloodgood, M. A.; Wu, L.; Verheijen, M. A.; Vandalon, V.; Kessels, W. M. M.; Hofmann, J. P.; Bol, A. A. Edge-Site Nanoengineering of WS_2 by Low-Temperature Plasma-Enhanced Atomic Layer Deposition for Electrocatalytic Hydrogen Evolution. *Chem. Mater.* **2019**, *31*, 5104–5115. https://doi.org/10.1021/acs.chemmater.9b01008.

(43) Shard, A. G. Detection Limits in XPS for More than 6000 Binary Systems Using Al and Mg Kα X-Rays. *Surf. Interface Anal.* **2014**, *46*, 175–185. https://doi.org/10.1002/sia.5406.

(44) Mahler, B.; Hoepfner, V.; Liao, K.; Ozin, G. A. Colloidal Synthesis of 1T-WS_2 and 2H-WS_2 Nanosheets: Applications for Photocatalytic Hydrogen Evolution. *J. Am. Chem. Soc.* **2014**, *136*, 14121–14127. https://doi.org/10.1021/ja506261t.

(45) Gladfelter, W. L. Selective Metalization by Chemical Vapor Deposition. *Chem. Mater.* **1993**, *5*, 1372–1388. https://doi.org/10.1021/cm00034a004.

(46) Parsons, G. N. Functional Model for Analysis of ALD Nucleation and Quantification of Area-Selective Deposition. *J. Vac. Sci. Technol. A* **2019**, *37*, 020911. https://doi.org/10.1116/1.5054285.

(47) Balasubramanyam, S.; Bloodgood, M. A.; van Ommeren, M.; Faraz, T.; Vandalon, V.; Kessels, W. M. M.; Verheijen, M. A.; Bol, A. A. Probing the Origin and Suppression of Vertically Oriented Nanostructures of 2D WS_2 Layers. *ACS Appl. Mater. Interfaces* **2020**, *12*, 3873-3885. https://doi.org/10.1021/acsami.9b19716.

(48) Berkdemir, A.; Gutiérrez, H. R.; Botello-Méndez, A. R.; Perea-López, N.; Elías, A. L.; Chia, C.-I.; Wang, B.; Crespi, V. H.; López-Urías, F.; Charlier, J.-C.; et al. Identification of Individual and Few Layers of WS_2 Using Raman Spectroscopy. *Sci. Rep.* **2013**, *3*, 1755. https://doi.org/10.1038/srep01755.

(49) Thripuranthaka, M.; Kashid, R. V.; Sekhar Rout, C.; Late, D. J. Temperature Dependent Raman Spectroscopy of Chemically Derived Few Layer MoS_2 and WS_2 Nanosheets. *Appl. Phys. Lett.* **2014**, *104*, 081911. https://doi.org/10.1063/1.4866782.

(50) Song, J.; Park, J.; Lee, W.; Choi, T.; Jung, H.; Lee, C. W.; Hwang, S.; Myoung, J. M.; Jung, J.; Kim, S.-H.; et al. Layer-Controlled, Wafer-Scale, and Conformal Synthesis of Tungsten Disulfide Nanosheets Using Atomic Layer Deposition. *ACS Nano* **2013**, *7*, 11333–11340. https://doi.org/10.1021/nn405194e.

TOC FIGURE